Microsc. Microanal. 19, 745–750, 2013
doi:10.1017/S1431927613000238

Microscopy AND Microanalysis

A Direct and Quantitative Three-Dimensional Reconstruction of the Internal Structure of Disordered Mesoporous Carbon with Tailored Pore Size

Juan Balach,[1] Flavio Soldera,[2] Diego F. Acevedo,[1] Frank Mücklich,[2] and César A. Barbero[1,*]

[1]*Programa de Nanomateriales y Mesomateriales, Universidad Nacional de Río Cuarto, Agencia Postal No 3, 5800 Río Cuarto, Argentina*
[2]*Department Materials Science, Saarland University, Campus D3.3, 66123 Saarbrücken, Germany*

Abstract: A new technique that allows direct three-dimensional (3D) investigations of mesopores in carbon materials and quantitative characterization of their physical properties is reported. Focused ion beam nanotomography (FIB-nt) is performed by a serial sectioning procedure with a dual beam FIB-scanning electron microscopy instrument. Mesoporous carbons (MPCs) with tailored mesopore size are produced by carbonization of resorcinol-formaldehyde gels in the presence of a cationic surfactant as a pore stabilizer. A visual 3D morphology representation of disordered porous carbon is shown. Pore size distribution of MPCs is determined by the FIB-nt technique and nitrogen sorption isotherm methods to compare both results. The obtained MPCs exhibit pore sizes of 4.7, 7.2, and 18.3 nm, and a specific surface area of ca. 560 m^2/g.

Key words: focused ion beam (FIB), nanotomography, mesoporous carbon, image analysis, pore size distribution

Introduction

Porous carbon materials have a wide use in many fields, which highlights its potential for technological applications such as active material for the storage of energy in supercapacitors and support for catalysts (Frackowiak & Béguin, 2001; Moreno-Castilla & Maldonado-Hódar, 2005). Important parameters of such materials are the large specific surface area as well as the tailored pore structure. Mercury porosimetry and gas sorption isotherm methods are frequently used to obtain information on the amount of surface area and/or the average pore size. However, an image of the porous materials is not provided by these techniques. Some techniques, such as transmission electron microscopy, small-angle X-ray scattering, and small-angle neutron scattering, can give a picture of the ordered porous materials; however, these methods fail when it is necessary to obtain a detailed three-dimensional (3D) image of disordered porous carbon (e.g., activated carbon, which is a common material). In the last decade the focused ion beam-nanotomography (FIB-nt) technique has been used to describe 3D topological features in different materials (Inkson et al., 2001; Holzer et al., 2004; Holzer et al., 2006; Konrad et al., 2006; Münch et al., 2006; Uchic et al., 2006; Wilson et al., 2006; Velichko et al., 2007; Balach et al., 2012). The 3D characterization of materials is based on a serial sectioning procedure with a FIB/scanning electron microscopy (SEM) dual beam system. Serial FIB cross sections are produced cutting through the selected volume by milling steps, and the sectioned surface can be imaged with an SEM. The analysis is performed automatically using a scripting routine. Its resolution depends on the precision of individual FIB cuts and on the resolution of the SEM images (Lasagni et al., 2008). Recently, Zhang et al. (2011) studied the porosity and permeability of a shale rock by combining 3D images obtained by the FIB-nt technique and advanced image analysis algorithms. The combination of the techniques mentioned above can potentially be applicable to a wide range of porous material.

Herein, FIB-nt will be employed to obtain a visual 3D morphology representation of nonordered mesoporous carbon and to accurately characterize their structural parameters such as connectivity of pores and pore size distribution for three different carbon samples. Pore size distribution of carbon samples is also determined by the nitrogen adsorption-desorption isotherm method to validate results obtained with the FIB-nt technique. The strength of FIB-nt is that it provides a detailed 3D picture of the pore size, distribution, and connectivity, which is necessary to assess the usefulness of carbon materials for technological applications.

Received June 9, 2012; accepted December 6, 2012
*Corresponding author. E-mail: cbarbero@exa.unrc.edu.ar

Materials and Methods

Synthesis of Hierarchical Porous Carbons

Precursor gels were synthesized by sol-gel polycondensation of resorcinol (R) with formaldehyde (F) in the presence of surfactant (Balach et al., 2012). In this study, sodium carbonate (C) and cationic surfactant, cetyltrimethylammonium bromide (CTAB), were used as a basic catalyst and a pore stabilizer, respectively. The precursor gel solutions were prepared mixing R (Fluka, Buchs, Switzerland), F (37 wt%, in an aqueous solution stabilized by 10% methanol) (Cicarelli), CTAB (BDH), Na_2CO_3 (Cicarelli, Santa Fé, Argentina), and deionized water (W). In all samples the molar ratio of R to F (R/F) was fixed at 0.5, the molar ratio of R to

sodium carbonate (R/C) was 600, and the ratio of R to W (R/W) was 0.5 g/cm^3. To study the influence of the conditions for sol-gel polycondensation on the porous structures of the carbon samples, the molar ratio of CTAB to R (CTAB/R) was varied from 0.08 to 0.12. The mixtures were stirred and heated over the Kraft temperature of the surfactant to promote the micellization. Then the samples were polymerized by heating at 70°C, in a closed system, for 24 h to obtain organic gels. The organic gels were dried at ambient pressure and room temperature for 3 days. Finally, the dried gels were converted into mesoporous carbons (MPCs) by carbonization under flowing argon at 800°C with a heating rate of 40°C/h and kept at 800°C for 1 h. The obtained samples were denoted as MPC-*x*, where *x* corresponds to the molar ratio of CTAB/R.

Physical Characterization

Nitrogen adsorption-desorption experiments were performed with a Quantachrome Instruments (Boynton Beach, FL, USA) Autosorb-iQ at liquid nitrogen temperature, and data analysis was performed with the ASiQwinv 1.11 software. The samples were degassed at 453 K for 12 h before measurements. Brunauer-Emmett-Teller (BET) surface area (S_{BET}) was calculated using the BET theory (Brunauer et al., 1938). The total pore volume (V_{tot}) was estimated from the amount adsorbed at relative pressure (P/P_0) of 0.984. Micropore surface area (S_{mic}) and micropore volume (V_{mic}) were deduced from the *t*-plot method. Micropore size distribution (d_{mic}) was calculated using the nonlinear density functional theory method (Ravikovitch & Neimark, 2001), assuming slit pore shape. Mesopore size distribution (d_{meso}) and mesopore volume (V_{meso}) were determined by the Barrett-Joyner-Halenda (BJH) method (Gregg & Sing, 1982) from desorption branch of the isotherm.

Morphological Characterization

Carbon morphology was observed using a SEM. A dual beam workstation (FEI Helios Nanolab 600; FEI Company, Hillsboro, OR, USA) equipped with a FIB column employing a gallium liquid metal ion source, combined with a field emission gun SEM was used. The SEM column was used for general imaging, and the FIB column was used for cross-section preparation.

Three-Dimensional Reconstruction and Quantitative Analysis

The general principle of FIB-nt consists of milling the material with high precision to produce a cross section, and the sectioned surface can be imaged with the SEM. Afterward, serial sections of the cross section, with a defined distance between slices, are successively milled with FIB and imaged with SEM. Details on this technique are described elsewhere (Phaneuf, 1999; Holzer et al., 2004; Lasagni et al., 2008). Before making a cross section in the sample, a layer of Pt was deposited, induced by the electron beam, upon the area of investigation to avoid undesired ion-induced erosion of the surface and edge of the cross section to help reduce curtaining effects (Giannuzzi & Stevie, 2005). During the sectioning process, the surface sample (*x*-*z* plane) was oriented perpendicularly to the ion beam (*y*-direction). The *x*-*y* plane corresponds to the front view of the cross sections, and the SEM images were taken using a tilt angle of 52°. Secondary electron images for tomography were done with a voltage of 5 kV, a nominal current of 86 pA, and a dwell time of 60 μs. Increasing the voltage improves the focus of the image due to better depth of focus, but the electron interaction volume with the sample increases as well. Five kilovolts was chosen for imaging to achieve a compromise between the depth of penetration and chromatic aberration effects while retaining spatial resolution. A through-the-lens detector was used. The milling process was performed with an ion beam current of 27 pA at 30 kV. The sectioning and imaging process was automatically performed using the FEI SliceAndView G2 software. The milling of each 10-nm-thick slice of 2.66 $\times$ 4 μm^2 (width $\times$ height) required 20 s, and a subsequent acquisition of the SEM image required about 40 s. A stack of 100 images can be acquired within 2 h. This time takes into account the corrections for sample drift done using ion beam induced secondary electron images after each slice and changes in the focal depth during sectioning procedure, which was done manually by interrupting the procedure after several slices.

Data processing and 3D reconstruction of structures from the image stack collected during the serial sectioning procedure were done using the 3D reconstruction package Amira® 5.2 software. The SEM images were aligned using the Pt-sample interface, and the segmentation of the image stack was carried out afterward. In this 3D tomography study, the samples were reconstructed from 25 slices obtained at a thickness of 10 nm per slice. The volume analyzed was defined by 500 nm in the *x*-direction, 500 nm in the *y*-direction, and 250 nm in the *z*-direction. Voxel size was calculated in *x* and *y* from resolution of the SEM images and in *z* from the distance between slices. The voxel size was 3.57 $\times$ 3.62 $\times$ 10 nm^3. For further quantitative analyses, the software system Modular Algorithms for Volume Images (MAVI) was employed (Nagel et al., 2000; Ohser & Mücklich, 2000).

Results and Discussion

Textural Properties

Nitrogen sorption measurements and pore size distribution of MPCs prepared with different CTAB/R ratios are shown in Figure 1, and the results of physical properties are summarized in Table 1. According to the IUPAC classification, the nitrogen adsorption for all samples belongs to a type IV isotherm (see Fig. 1a), indicating the presence of mesoporous in the carbon samples. There is a clear trend that an increase in CTAB/R ratio increased the mesopore size (see Fig. 1b). These results indicate that physical properties of the carbon materials can be tailored by controlling the CTAB concentration in the initial stage of the R-F polymer-

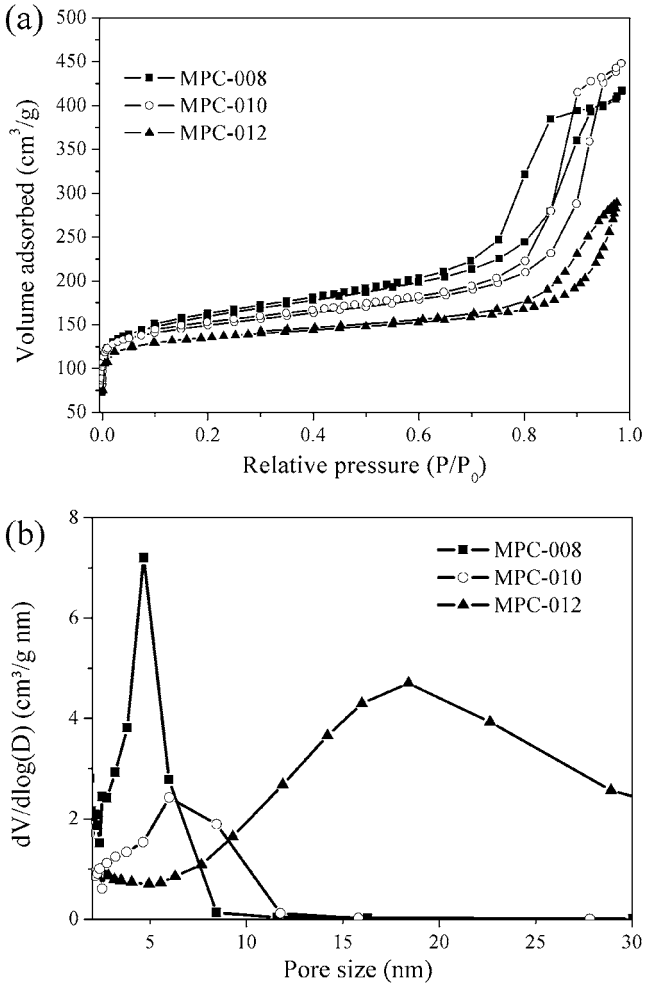

Figure 1. (**a**) Nitrogen sorption isotherms of MPCs prepared with different CTAB/R ratios. (**b**) BJH pore size distribution plots.

ization process. However, the three samples analyzed have a similar micropore surface area and micropore size, so the increase in mesopore size yields a decrease in surface area.

Surface and Internal Morphology

Surface morphology of MPCs was examined by SEM. Figure 2 shows a significant surface porosity in all carbon samples and also that the pore size increases with an increase in CTAB/R ratio. This behavior is consistent with the results obtained by nitrogen sorption analysis. This means that pore size of the MPCs could be controlled by varying the concentration of the CTAB.

To observe the porous structures inside MPCs, cross sections were prepared by FIB and imaged by SEM. As shown in Figure 3, the images obtained reveal that the monolithic carbons have homogeneous porosity throughout the material. Also, it is clearly visible that pore size increased upon increasing the molar ratio CTAB/R. However, we are only observing a cross section, and therefore it is not possible to determine for these pores if they are closed or not passing through the whole carbon material. To evaluate the depth and the connectivity of the pores, FIB-nt was used.

Three-Dimensional Representation and Quantitative Analysis

Through automation of the successive FIB milling of slices and SEM imaging, a stack of images were processed to obtain a 3D representation of MPC samples. Figure 4 shows a stack of images obtained after serial sectioning of sample MPC-012. Based on these serial sections, 3D reconstructions were performed to produce 3D images of porous carbon materials. Figure 5 shows different 3D images, where analyzed volume of the samples MPC-008, MPC-010, and MPC-012 can be observed in Figures 5a–5c, respectively. The size of each analyzed volume corresponds to a parallelepiped(?) with $[xyz] = 500 \times 500 \times 250$ nm^3. Figures 5d–5f correspond to the 3D reconstruction of the volumes shown in Figures 5a–5c; in these 3D images the pore space is highlighted. The main difficulties of segmenting images of porous samples obtained by SEM relay in distinguishing the real cut cross section from the ground of the pores. That is, a plane that is some nanometers back from the real cross section. Therefore, an automatic segmentation is almost impossible. In this case, a manual segmentation was done with some help by the grayscale-threshold tool. Any curtaining effect (as appears for instance in Fig. 3c) did not affect the segmentation because this was done manually and the operator took this in account. As it can be seen in Figures 5d–5f, the pore size increases when the CTAB/R ratio is larger. The fashion pore structure seems to be similar in all of the samples. Figures 5e and 5f show that samples MPC-010 and MPC-012 present a good connection between pores. It is also possible to observe that the connected network of pores increases when the CTAB/R ratio is increased. In the case of MPC-008, there are a few insolated pores. To obtain more information from the 3D representations, a quantitative analysis was also performed.

Table 1. Physical Properties of MPCs.*

Sample	S_{BET} (m^2/g)	S_{mic} (m^2/g)	V_{tot} (cm^3/g)	V_{meso} (cm^3/g)	V_{mic} (cm^3/g)	d_{mic} (nm)	d_{meso} (nm)
MPC-008	585	400	0.645	0.458	0.170	0.72	4.7
MPC-010	559	385	0.935	0.509	0.155	0.82	7.2
MPC-012	512	398	0.447	0.255	0.159	0.79	18.3

*S_{BET}, BET surface area; S_{mic}, micropore surface area; V_{tot}, total pore volume; V_{meso}, mesopore volume; V_{mic}, micropore volume, d_{mic}, micropore size distribution; d_{meso}, mesopore size distribution.

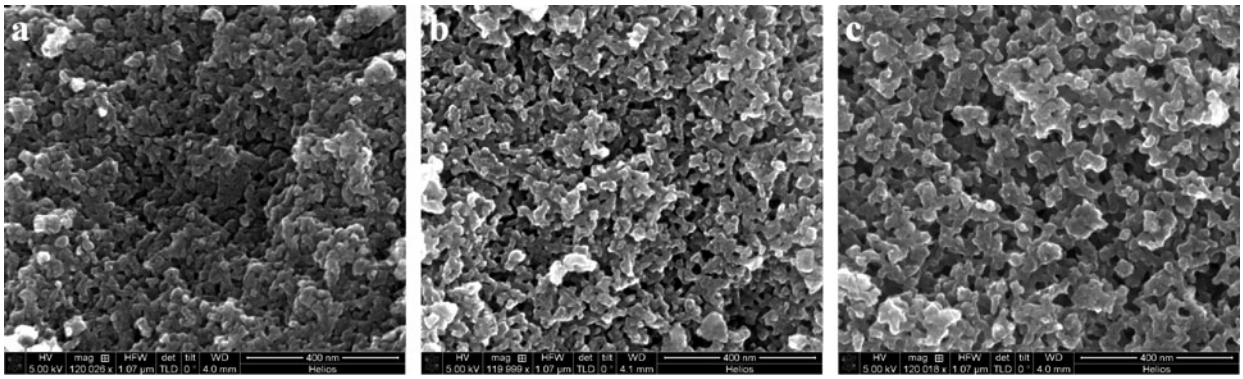

Figure 2. SEM images of the surfaces of MPCs prepared using different CTAB/R molar ratio: (**a**) MPC008, (**b**) MPC010, and (**c**) MPC012. Scale bars = 400 nm.

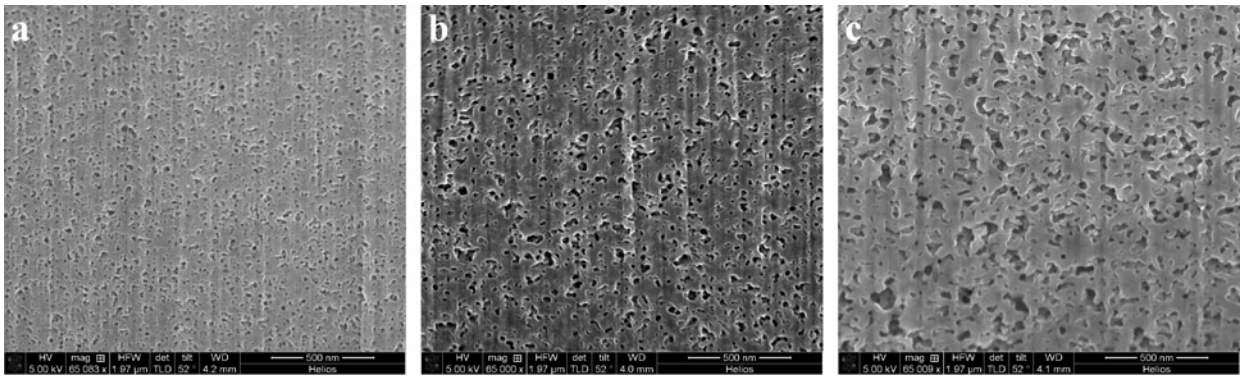

Figure 3. SEM cross section of MPCs with different pore sizes: (**a**) MPC008, (**b**) MPC010, and (**c**) MPC012. Scale bars = 500 nm.

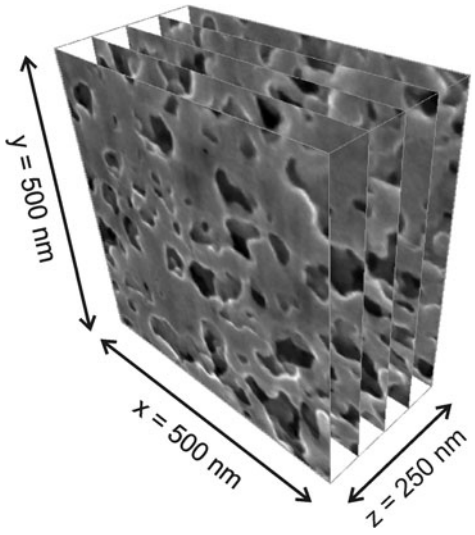

Figure 4. Stack of images produced with FIB-nt from sample MPC012. The *x*-direction is parallel to the ion beam.

The 3D characterization was carried out with the software MAVI. The total analyzed volume (V_T) of material was 0.0625 μm^3. Structural parameters of the pores such as surface area (S), pore volume (V), Euler number (χ), total porosity (P), and pore size distribution (PSD) were determined. The results are shown in Table 2. The Euler number is a topological characteristic, which describes the spatial connectivity and is calculated in the 3D space (Russ & Dehoff, 2000). Here, the Euler number with positive and negative values represents the uncompleted and completed connected network, respectively.

The Euler number of MPC-008, which is positive, indicates that the sample has a large number of insolate pores. While the Euler numbers of MPC-010 and MPC-012 are negative. This means that these samples have a well-connected network of pores, principally when the CTAB/R ratio is 0.12. As can be observed in Table 2, PSD values correlated well with the mesopore size distribution obtained by the BJH method (see Table 1). These results suggest that only the mesopore is revealed by FIB-nt, while resolution of the SEM instrument is not sufficient for access to pores with a diameter below 2 nm.

An important field of application of porous carbon is its use as support material in fuel cell. Production of electric power by a fuel cell requires the transport of reactant gases such as hydrogen to the anode and oxygen to the cathode. The interaction of the gas with the electrode may affect performance of the fuel cell, and for that reason it is important to know the pore size and connectivity between pores. The detailed 3D topographic image rendered by FIB-nt could be quite helpful to ascertain accessibility of the carbon surfaces by the reactant in the supercapacitor.

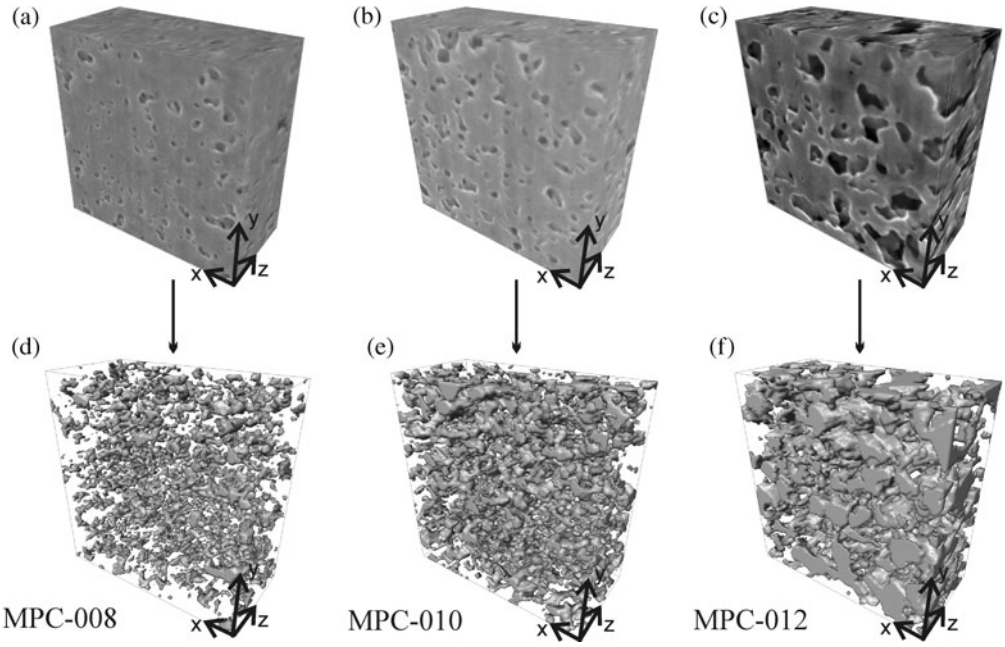

Figure 5. (**a–c**) Sections of MPCs analyzed and (**d–f**) 3D reconstruction of MPC-008, MPC-010, and MPC-012. The solid material describes the pores. Volume analyzed is $[xyz] = 500 \times 500 \times 250$ nm^3.

Conclusions

The use of CTAB as a porosity stabilizer in the reaction media during the sol-gel polycondensation of R with F produces the formation of both micropores and mesopores. FIB-nt is able to reveal the 3D shape, distribution, and connectivity of mesopores in carbon materials. Using 3D reconstruction and analysis software, it was possible to visualize and study nonordered pore morphology and quantitatively characterize their physical properties. Mesopore size rendered by the FIB-nt technique correlates well with nitrogen adsorption isotherm measurements. This means that it is possible to use the FIB-nt technique as a new tool for the visual and quantitative analysis of porous carbon materials. Moreover, given that the porous structure of synthetic disordered porous carbons can be controlled from synthetic conditions (Bruno et al., 2010), studies of the porosity and connectivity of the pores via characterization using FIB-nt measurement will allow the choice of the best carbon material for technological applications, such as fuel cell electrodes, lithium batteries, electric double layer supercapacitors, and catalyst support.

Table 2. Surface Area (S), Pore Volume (V), Euler Number (ε), and Pore Size Distribution (PSD) Determined from the 3D Reconstructions of Figure 4 for the Different MPC Samples.*

Sample	S (μm^2)	V (μm^3)	ε	PSD (nm)
MC-008	1.446	0.0048	975	4
MC-010	2.564	0.0118	−76	8
MC-012	2.597	0.0214	−436	14

*The total analyzed volume for all samples was 0.0625 μm^3.

Acknowledgments

This work was funded by FONCYT, CONICET, MinCyt (Cordoba) SECYT-UNRC, and NANOCOM Network (IRSES, 7th Framework Program of the European Commission). J. Balach thanks CONICET for a graduate research fellowship. C. Barbero and D. Acevedo are permanent research fellows of CONICET. F. Soldera and F. Mücklich thank the EFRE Funds of the European Commission for support of activities within the AME-Lab project. The authors would like to thank project partners S. Suarez and F. Miguel for their help with 3D image analyses and K. Sapag and J. Villarroel Rocha for the nitrogen sorption measurements.

References

Balach, J., Miguel, F., Soldera, F., Acevedo, D.F., Mücklich, F. & Barbero, C.A. (2012). A direct and quantitative image of the internal nanostructure of nonordered porous monolithic carbon using FIB nanotomography. *J Microsc* **246**(3), 274–278.

Brunauer, S., Emmett, P.H. & Teller, E. (1938). Adsorption of gases in multimolecular layers. *J Am Chem Soc* **60**(2), 309–319.

Bruno, M.M., Cotella, N.G., Miras, M.C. & Barbero, C.A. (2010). A novel way to maintain resorcinol-formaldehyde porosity during drying: Stabilization of the sol-gel nanostructure using a cationic polyelectrolyte. *Colloid Surf A* **362**(1–3), 28–32.

Frackowiak, E. & Béguin, F. (2001). Carbon materials for the electrochemical storage of energy in capacitors. *Carbon* **39**(6), 937–950.

Giannuzzi, L.A. & Stevie, F.A. (2005). *Introduction to Focused Ion Beams: Instrumentation, Theory, Techniques and Practice*. Berlin: Springer.

Gregg, S.J. & Sing, K.S.W. (1982). *Adsorption, Surface Area and Porosity*. London: Academic Press.

Holzer, L., Indutnyi, F., Gasser, P.H., Münch, B. & Wegmann, M. (2004). Three-dimensional analysis of porous $BaTiO_3$ ceramics using FIB nanotomography. *J Microsc* **216**(1), 84–95.

Holzer, L., Muench, B., Wegmann, M., Gasser, P. & Flatt, R.J. (2006). FIB-nanotomography of particulate systems—Part I: Particle shape and topology of interfaces. *J Am Ceram Soc* **89**(8), 2577–2585.

Inkson, B.J., Mulvihill, M. & Möbus, G. (2001). 3D determination of grain shape in a FeAl-based nanocomposite by 3D FIB tomography. *Scripta Mater* **45**(7), 753–758.

Konrad, J., Zaefferer, S. & Raabe, D. (2006). Investigation of orientation gradients around a hard Laves particle in a warm-rolled Fe_3Al-based alloy using a 3D EBSD-FIB technique. *Acta Mater* **54**(5), 1369–1380.

Lasagni, F., Lasagni, A., Engstler, M., Degischer, H.P. & Mücklich, F. (2008). Nano-characterization of cast structures by FIB-tomography. *Adv Eng Mater* **10**(1–2), 62–66.

Moreno-Castilla, C. & Maldonado-Hódar, F.J. (2005). Carbon aerogels for catalysis applications: An overview. *Carbon* **43**(3), 455–465.

Münch, B., Gasser, P., Holzer, L. & Flatt, R. (2006). FIB-nanotomography of particulate systems—Part II: Particle recognition and effect of boundary truncation. *J Am Ceram Soc* **89**(8), 2586–2595.

Nagel, W., Ohser, J. & Pischang, K. (2000). An integral-geometric approach for the Euler–Poincaré characteristic of spatial images. *J Microsc* **198**(1), 54–62.

Ohser, J. & Mücklich, F. (2000). *Statistical Analysis of Microstructures in Materials Science*. New York: John Wiley.

Phaneuf, M.W. (1999). Applications of focused ion beam microscopy to materials science specimens. *Micron* **30**(3), 277–288.

Ravikovitch, P.I. & Neimark, A.V. (2001). Characterization of nanoporous materials from adsorption and desorption isotherms. *Colloid Surf A* **187–188**, 11–21.

Russ, J.C. & Dehoff, R. (2000). *Practical Stereology*. New York: Kluwer Academic/Plenum Publishers.

Uchic, M.D., Groeber, M.A., Dimiduk, D.M. & Simmons, J.P. (2006). 3D microstructural characterization of nickel superalloys via serial-sectioning using a dual beam FIB-SEM. *Scripta Mater* **55**(1), 23–28.

Velichko, A., Holzapfel, C. & Mücklich, F. (2007). 3D Characterization of graphite morphologies in cast iron. *Adv Eng Mat* **9**(1–2), 39–45.

Wilson, J.R., Kobsiriphat, W., Mendoza, R., Chen, H.-Y., Hiller, J.M., Miller, D.J., Thornton, K., Voorhees, P.W., Adler, S.B. & Barnett, S.A. (2006). Three-dimensional reconstruction of a solid-oxide fuel-cell anode. *Nat Mater* **5**(7), 541–544.

Zhang, S., Klimentidis, R.E. & Barthelemy, P. (2011). Porosity and permeability analysis on nanoscale FIB-SEM 3D imaging of shale rock. In *25th International Symposium of the Society of Core Analysts*, pp. 1–12. Austin, TX: Society of Core Analysts.